ADVANCED OPTICAL MATERIALS
www.advopticalmat.de

# Extreme Nonreciprocity in Metasurfaces Based on Bound States in the Continuum

*Luis Manuel Máñez-Espina,* Ihar Faniayeu, Viktar Asadchy, and Ana Díaz-Rubio*

**Nonreciprocal devices, including optical isolators, phase shifters, and amplifiers, are pivotal for advanced optical systems. However, exploiting natural materials is challenging due to their weak magneto-optical (MO) effects, requiring substantial thickness to construct effective optical devices. In this study, it is demonstrated that subwavelength metasurfaces supporting bound states in the continuum (BICs) and made of conventional ferrimagnetic material can exhibit strong nonreciprocity in the Faraday configuration and near-unity magnetic circular dichroism (MCD). These metasurfaces enhance the MO effect by 3–4 orders of magnitude compared to a continuous film of the same material. This significant enhancement is achieved by leveraging Huygens' condition in the metasurface whose structural units support paired electric and magnetic dipole resonances. The multi-mode temporal coupled mode theory (CMT) is developed for the observed enhancement of the MO effect, and the findings with the full-wave simulations are confirmed.**

## 1. Introduction

In the race for the miniaturization of optical devices, a wide class of electromagnetic structures named metasurfaces arose in the last decade as one of the most prominent solutions. Optical metasurfaces are 2D arrays of nano-inclusions with a sub-wavelength thickness that are engineered to manipulate light at will.[1–4] Theoretically, if the inclusions, known as meta-atoms, are properly designed, almost any response that does not violate fundamental laws of physics could be achieved for these structures. One of the important industrial applications of metasurfaces is the design of nonreciprocal optical components such as isolators. In order to achieve optical isolation, a necessary condition is that the device must be nonreciprocal.[5] Traditionally, nonreciprocity has been implemented using magneto-optical (MO) materials such as ferrites.[6] Nevertheless, MO effects are very weak in the optical regime[7] and must be enhanced with proper techniques for designing compact nonreciprocal devices. Recently, there have been multiple techniques suggested to achieve an enhancement of MO effects in a subwavelength structure: magnetophotonic crystals,[8–11] coupled surface-plasmon polaritons,[12–14] magnetic Weyl semimetals,[15] multiple layer systems,[16] and resonant all-dielectric metasurfaces.[17–21] Although these studies achieve a high enhancement, the resonant properties of the structures considered do not allow ultra-high quality factors that would enable higher interaction times between light and the MO material.[18] An attractive path toward designing compact optical nonreciprocal components is based on bound states in the continuum (BICs) which, if properly engineered, enable almost non-leaky resonances that increase the interaction time and the field concentration in the materials of the resonant structure. BICs in metasurfaces have been widely researched in the last few years.[22] In electromagnetism, these bound states with infinite lifetimes are discrete solutions of the Maxwell equations embedded in a continuum of leaky modes and inaccessible by incident external radiation.[23] Their useful realization comes in the form of quasi-BICs, which are perturbed BICs that have turned into accessible leaky modes with extreme quality factors (ultra-long but finite lifetimes).[24,25] Over recent years, metasurfaces that use these states have been proposed to enhance different effects: circular dichroism,[26–28] absorption,[29,30] and more. Furthermore, BICs can be classified into different categories depending on their formation nature.[23] Particularly interesting and relatively easy to exploit are the symmetry-protected BICs (SP-BICs),[31] which have been precisely characterized by their group representations.[32–34] Specifically, SP-BICs are inaccessible states that do not couple to the plane wave modes because of symmetry incompatibility between incident excitation and structural symmetries.[25] Several metasurface designs with enhanced MO effects were recently proposed based on BICs.[35–37] However, they were either limited to the THz range where magneto-optical

L. M. Máñez-Espina, A. Díaz-Rubio
Nanophotonics Technology Center
Universitat Politècnica de València
Camí de Vera s/n, Valencia 46022, Spain
E-mail: lmmaeesp@teleco.upv.es
I. Faniayeu
Department of Physics
University of Gothenburg
Origovägen 6B, Gothenburg 41296, Sweden
V. Asadchy
Department of Electronics and Nanoengineering
Aalto University
Maarintie 8, Espoo 02150, Finland

The ORCID identification number(s) for the author(s) of this article can be found under https://doi.org/10.1002/adom.202301455



**DOI: 10.1002/adom.202301455**

effects are relatively strong even in natural materials,[35] or based on nonrealistic materials (exhibiting no dissipation loss),[37] or exhibited relatively weak MO properties (in ref. [36], the reported Faraday rotation was in the order of 12 mrad). More importantly, in none of these works, a comprehensive theoretical explanation of the MO enhancement mechanism was given, which is essential for optimizing the performance of the structure and reaching the maximum strength of the effect.

In this work, we present a metasurface made of ferrimagnetic material that simultaneously supports BICs with electric and magnetic nature. We delve into the physical phenomena in the structure and develop a phenomenological multi-mode temporal coupled mode theory (CMT)[38,39] to serve as a recipe for the design of optical metasurfaces exhibiting maximum MO effects for the given materials being used. We demonstrate that by exploiting a pair of even and odd resonances in the metasurface unit cell (so-called Huygens' pair,[40]) it is possible to obtain nearly unit magnetic circular dichroism (MCD) in a simple geometry with conventional material (Bi3YIG) being used. Using this recipe, we design a nonreciprocal metasurface with a near-unit MCD that behaves as a nonreciprocal device for circularly polarized light, allowing a certain handedness to be transmitted when propagating in the forward direction and blocking it for backward illumination. This phenomenon would be referred to as partial isolation. If surrounded by two polarizers,[41] such a structure would operate as an optical isolator in transmission.

## 2. Metasurface Design

The metasurface design will follow a similar topology to that of refs. [41,42], where they described an array of dielectric nanodisks distributed in a squared lattice in a checkerboarded fashion with an asymmetry in diameter between nearest neighbors. However, in the present scenario, we consider the nanodisks to be made of ferrimagnetic material Bi3YIG experimentally characterized in ref. [43]. The metasurface geometry is shown in **Figure 1**. Its geometrical parameters are $l$ for the unperturbed diameter of the nanodisks, $w$ for the squared lattice constant, $h$ for the height of the nanodisks, and $\Delta$ for the difference in diameter between nearest neighbors. The diameters for the nanodisks are defined as $l_a = l + \Delta/2$ and $l_b = l - \Delta/2$. For simplicity of the analysis, we assume the metasurface to be surrounded by air from both sides. It is worth noticing that the same physics applies to the scenario when the metasurface is immersed inside some background dielectric material (for that, merely the permittivity of the nanodisks should be scaled up accordingly). For the scenario where the metasurface is located on top of a dielectric substrate, mirror symmetry would be broken, making the CMT analysis somewhat more involved.[44]

The material of the nanodisks is magnetized by a bias static magnetic field applied along the $+z$-axis, which results in its antisymmetric permittivity tensor of the form [6]

$$\bar{\bar{\varepsilon}}(\omega, \mathbf{H}_0) = \begin{pmatrix} \varepsilon_{xx}(\omega) & j\varepsilon_{xy}(\omega, \mathbf{H}_0) & 0 \\ -j\varepsilon_{xy}(\omega, \mathbf{H}_0) & \varepsilon_{xx}(\omega) & 0 \\ 0 & 0 & \varepsilon_{zz}(\omega) \end{pmatrix} \quad (1)$$

where $\varepsilon_{xx} = \varepsilon_{1r} - j\varepsilon_{1i}$ and $\varepsilon_{xy} = \varepsilon_{2r} - j\varepsilon_{2i}$ are complex permittivities and $\mathbf{H}_0$ denotes an external magnetic field along the $z$-axis.

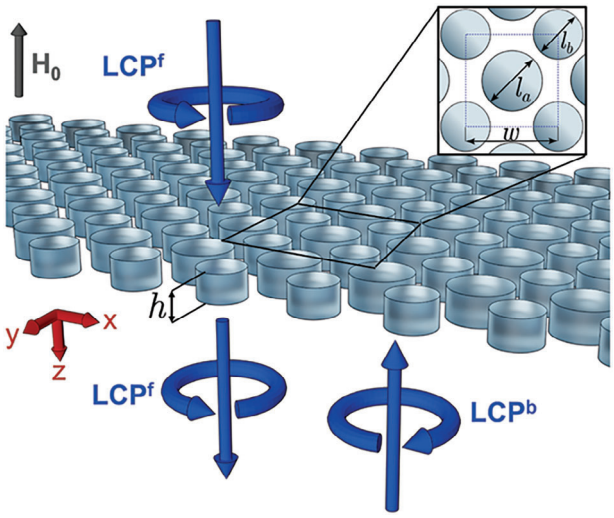


**Figure 1.** Schematic of the nonreciprocal metasurface exhibiting one-way transmission for circularly polarized light. The inset depicts the unit cell with the in-plane geometrical parameters. The neighboring nanodisks have slightly different diameters $l_a$ and $l_b$, and are arranged in checkerboard order. The LCP plane wave is labeled as "f" (forward) and "b" (backward). The external magnetic bias necessary to break reciprocity is shown at the top left of the figure.

Here we use the $e^{j\omega t}$ convention for temporal field evolution. Permittivity component $\varepsilon_{xy}$ is assumed to be a linear function of $\mathbf{H}_0$. Moreover, saturation is achieved in Bi3YIG with a field of 1.2 T.[43]

When $\varepsilon_{xy} = 0$ and $\varepsilon_{xx} = \varepsilon_{1r}$, the structure shown in Figure 1 is known to hold quasi-BICs resonant modes at normal incidence due to the mismatch in diameter between nanodisks.[41,42] The resonant modes of the metasurface are those shown in **Figure** 2a,b, obtained using the commercial FEM simulator COMSOL Multiphysics. These two modes correspond to the scenarios where the nanodisks acquire electric and magnetic dipole polarizations, respectively. These modes remain inaccessible for normal plane-wave incidence in the metasurface without geometrical perturbations (i.e., $\Delta = 0$). They are SP-BICs,[31] and their origin is due to the symmetries of the structure and can be explained in several ways. The most intuitive explanation can be done in terms of induced dipoles. A checkerboarded array of nanodisks can be thought of as a superposition of two sublattices, in this case, each holding a magnetic/electric dipole moment, but with a $\pi$ relative phase between wave oscillations in the two lattices. In the unperturbed case, the superposition of both lattices cancels the far-field radiation and forms an SP-BIC. In the perturbed case, the size of the nearest neighbor is altered, and the electric/magnetic dipoles are not identical. This geometrical mismatch induces a difference in amplitude and/or phase, enabling a non-perfect destructive superposition of scattered waves and creating a high-$Q$ resonance, that is, a quasi-BIC. When the perturbed metasurface supporting this type of resonant mode is illuminated by a linearly polarized wave, the interaction of the incident field and the resonant structure will produce two peaks in the transmission spectra, as shown in Figure 2c. These two peaks correspond to the resonance conditions of the two sub-lattices of dipole moments. The positions and the widths of the transmission peaks are closely related to

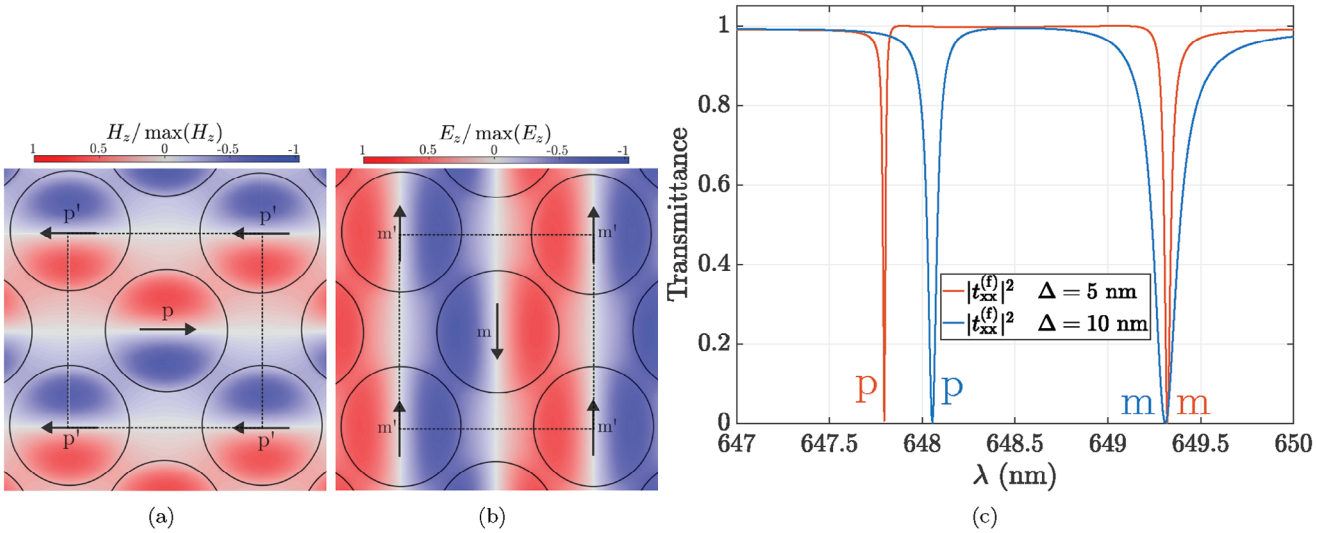


**Figure 2.** Resonant properties of the metasurface without external magnetic bias. Total field supported by the structure when $\Delta = 5$ and 10 nm, $l = 270$ nm, $w = 430$ nm, $h = 135.2$ nm, $\varepsilon_{xy} = 0$, and $\varepsilon_{xx} = \varepsilon_{1r}$ in the plane $z = 0$ (cutting-plane in the middle of the nanodisks). a) Electric dipole mode at $\lambda = 647.73$ nm and b) magnetic dipole mode at $\lambda = 649.30$ nm in the case where $\Delta = 5$ nm. The lattice cell is depicted with a dashed line. The dipole direction is shown with arrows. c) Transmittance of the metasurface without magnetic bias and dissipation losses. The asymmetry in diameter is proportional to the width of the resonance. The magnetic resonance width is greater than the electric dipole resonance. There is a noticeable shift in the electric dipole resonance frequency when $\Delta$ is changed.

the asymmetry of the structure quantified by the parameter $\Delta$. The resonant mode that appears at a lower wavelength is the electric dipole. As expected, the width of the resonant modes increases with the parameter $\Delta$ as the structure becomes more asymmetric. It is also interesting to notice that because the parameter $\Delta$ is directly related to the radius of the nanodisks, it has a larger impact on the position of the resonance frequency of the electric dipole.

In a more formal mathematical fashion, the BIC formation phenomenon can be explained by using group theory techniques. In the case of $\Delta = 0$, $\varepsilon_{xx} = \varepsilon_{1r}$, and $\varepsilon_{xy} = 0$, the cell and point symmetries are $C_{4v}$ and $C_2$ with two additional mirror planes (see Section S2, Supporting Information). As it is known, the eigenmodes of a periodic structure must satisfy the transformations given by an *irreducible representation* (IRREP) of the structure's symmetry group.[33] There is a BIC when there is no coupling between the external excitation and the structure's eigenmode. The absence of coupling is due to the incompatibility between the symmetry restrictions of the resonant structure and the incoming plane wave's symmetries.[45] Introducing a geometrical perturbation (i.e., $\Delta \neq 0$) removes the $C_2$ symmetry and one of the mirror planes, Figure S3, Supporting Information. Without them, the eigenmode symmetry is partially broken, and the coupling is enabled. The state is now referred to as a quasi-BIC. For this reason, the symmetry-protected label we used to refer to these BICs is now apparent. The structure behaves exactly the same way with linear $y$-polarized light or $x$-polarized light due to the $C_{4v}$ symmetry that it still holds. Moreover, the cell symmetry $C_{4v}$ explains the degeneracy of the electric and magnetic modes that belong to the same $\Gamma_5$ 2D IRREP[32] (see Section S2, Supporting Information). Furthermore, these eigenmodes, shown in Figure 2a,b, transform according to the $\Gamma_5$ irreducible representation of the $C_{4v}$ group.[28]

With the introduction of a magnetic bias, but neglecting the losses ($\varepsilon_{xy} = \varepsilon_{2r}$ and $\varepsilon_{xx} = \varepsilon_{1r}$), both magnetic and electric dipolar resonances split. As an example of this behavior, **Figure 3** represents the transmission spectra for two different values of the parameter $\Delta$ when the structure is biased by a magnetic field that brings the garnet to saturation. Note that this analysis is done by neglecting the losses in the material. The degeneracy that emerged from the 2D $\Gamma_5$ IRREP is now broken by the non-equal

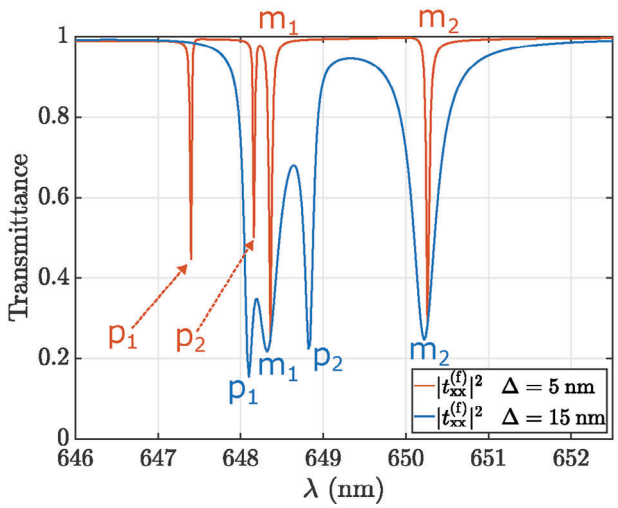


**Figure 3.** Resonant properties of the metasurface with external magnetic bias but without dissipation losses. The transmittance of the magnetically biased perturbed metasurface when $\Delta = 5$ nm and $\Delta = 15$ nm with the rest of the parameters with values $l = 270$ nm, $w = 430$ nm, and $h = 135.2$ nm. The electric dipoles $p_1$ and $p_2$ suffer a higher shift in wavelength than the magnetic dipole resonances $m_1$ and $m_2$.

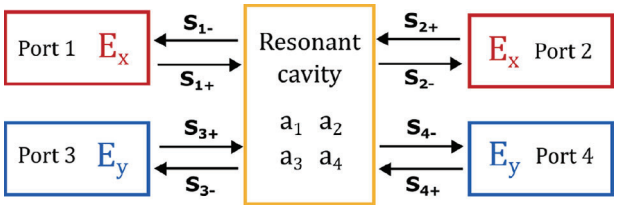


**Figure 4.** Schematics of the ports and the resonant metasurface for the CMT analysis.

off-diagonal components of the permittivity tensor (see Equation (1)). Due to the anisotropic and nonsymmetric nature of the material, mirror diagonal symmetries ($\sigma_{d1}$ and $\sigma_{d2}$) are broken. The point group of the structure is downgraded to $C_4$, which is the group that has the 90° rotation about the $z$-axis as its generator. The corresponding degenerate resonances split as their 2D IRREP ($\Gamma_5$ of $C_{4v}$) splits into two 1D IRREPs ($\Gamma_3$ and $\Gamma_4$ of $C_4$)[32] (see Section S2, Supporting Information). Furthermore, after the split, each pair of electric/magnetic dipole resonances will have one nondegenerated resonance coupling to a particular circular polarization, and the other coupling to the orthogonal circular polarization.[46]

In addition, the introduction of losses leaves the structure's symmetry unperturbed but limits the quality factors of the quasi-BICs, as pointed out in ref. [47]. Moreover, for the same values of Δ, the quality factor, and amplitude of the resonance will drop significantly. Nevertheless, losses in the material make possible such physical effects as the MCD and isolation.

## 3. Coupled Mode Theory Description

To better understand the physics behind the structure and as a guideline for the design of actual devices, we developed a theoretical model based on temporal CMT. More specifically, our model will consider the interaction of four ports (two ports for each linear polarization) and four resonant modes (two electric and two magnetic modes in the presence of the magnetic bias). Defining the ports of the structure as in **Figure 4**, where ports 1 and 2 account for the $x$-polarization channel and ports 3 and 4 form the $y$-polarization channel. The $C_4$ symmetry of the structure ensures that the scattering matrix (expressed in the linear-polarization basis) of the device has the form (Supporting Information)

$$\mathbf{S}_{\text{lin}} = \begin{pmatrix} r & t & r_{xy} & t_{xy} \\ t & r & t_{xy} & r_{xy} \\ -r_{xy} & -t_{xy} & r & t \\ -t_{xy} & -r_{xy} & t & r \end{pmatrix} \tag{2}$$

where $r$ and $t$ represent the reflection and transmission amplitude coefficients when the polarization state of the incident light is preserved (co-polarized coefficients), while $r_{xy}$ and $t_{xy}$ are the reflection and transmission coefficients when the polarization is changed (cross-polarized coefficients). The scattering matrix of the metasurface in the circular-polarization basis with basis vectors $\mathbf{e}_{\pm} = (\mathbf{e}_x \mp j\mathbf{e}_y)/\sqrt{2}$ has the form (Supporting Information)

$$\mathbf{S}_{\text{circ}} = \begin{pmatrix} r^{\text{f}}_{L-R} & t^{\text{b}}_{L-L} & 0 & 0 \\ t^{\text{f}}_{R-R} & r^{\text{b}}_{R-L} & 0 & 0 \\ 0 & 0 & r^{\text{f}}_{R-L} & t^{\text{b}}_{R-R} \\ 0 & 0 & t^{\text{f}}_{L-L} & r^{\text{b}}_{L-R} \end{pmatrix} = \begin{pmatrix} r_+ & t_+ & 0 & 0 \\ t_+ & r_+ & 0 & 0 \\ 0 & 0 & r_- & t_- \\ 0 & 0 & t_- & r_- \end{pmatrix} \tag{3}$$

where the superscripts "f" and "b" indicate forward ($+z$) or backward propagation ($-z$), and the subscripts "L" and "R" indicate left and right-handedness of circular polarization, respectively. The elements of the scattering matrices in the two different polarization bases are related as: $t_+ = t + jt_{xy}$, $r_+ = r + jr_{xy}$, $t_- = t - jt_{xy}$, and $r_- = r - jr_{xy}$. It is worth mentioning that in the circular-polarization basis, nonreciprocity does not lead to a nonsymmetric scattering matrix due to the way that the elements of the matrix are defined, as discussed in ref. [48]. Moreover, as Equation (3) shows, the notation chosen embraces the mathematical definition of the circular-polarization basis, uniquely defined by the sign between $x$ and $y$ components. Light-handedness implies a choice in nomenclature and frame of reference, as pointed out and widely discussed in ref. [49]. Using the sign in the relative phase between components as the defining factor leaves no doubt about what polarization we refer to. In any case, the convention used to relate both parts of Equation (3) is the one commonly used in engineering, where the time dependence is defined as $e^{j\omega t}$, and the observer's frame of reference points towards the direction of propagation to declare the handedness.

A phenomenological CMT model can be developed following the general coupled-mode equations[38] and assuming that the four orthogonal resonant modes present in the structure are characterized by their resonant frequencies $\omega^{\pm}_{m,e}$ and the decay rates $\gamma^{\pm}_{m,e}$. With this notation, the subscript refers to the nature of the resonance and its symmetry (magnetic and electric, respectively). The superscript relates to which circular polarization the resonance couples after splitting due to the external magnetic field. Modeling the losses in the material for each resonance by the coefficient $1/\tau^{\pm}_{m,e}$ and applying the conditions for energy conservation and mirror symmetry,[39] we obtain the final expressions for the $S$-matrix coefficients in the circular-polarization basis:

$$t_+ = t_d - \frac{\gamma^+_m (r_d + t_d)}{j(\omega - \omega^+_m) + \gamma^+_m + 1/\tau^+_m} + \frac{\gamma^+_e (r_d - t_d)}{j(\omega - \omega^+_e) + \gamma^+_e + 1/\tau^+_e} \tag{4}$$

$$t_- = t_d - \frac{\gamma^-_m (r_d + t_d)}{j(\omega - \omega^-_m) + \gamma^-_m + 1/\tau^-_m} + \frac{\gamma^-_e (r_d - t_d)}{j(\omega - \omega^-_e) + \gamma^-_e + 1/\tau^-_e} \tag{5}$$

$$r_+ = r_d - \frac{\gamma^+_m (r_d + t_d)}{j(\omega - \omega^+_m) + \gamma^+_m + 1/\tau^+_m} - \frac{\gamma^+_e (r_d - t_d)}{j(\omega - \omega^+_e) + \gamma^+_e + 1/\tau^+_e} \tag{6}$$

$$r_- = r_d - \frac{\gamma_m^-(r_d + t_d)}{j(\omega - \omega_m^-) + \gamma_m^- + 1/\tau_m^-} - \frac{\gamma_e^-(r_d - t_d)}{j(\omega - \omega_e^-) + \gamma_e^- + 1/\tau_e^-} \tag{7}$$

where $t_d$ and $r_d$ are the direct transmission and reflection coefficients. A more detailed derivation of these expressions is provided in Section S4, Supporting Information.

## 4. Maximization of Nonreciprocity and Magnetic Circular Dichroism

In this section, we derive the ideal conditions under which the metasurface with the aforementioned properties provides the highest (unitary) MCD and the highest isolation. MCD is conventionally defined in terms of the difference in absorptions for the two circular polarizations of light[50]

$$\mathrm{MCD} = \frac{\mathrm{A}_- - \mathrm{A}_+}{\mathrm{A}_- + \mathrm{A}_+} = \frac{(|\mathrm{t}_+|^2 - |\mathrm{t}_-|^2) + (|\mathrm{r}_+|^2 - |\mathrm{r}_-|^2)}{2 - (|\mathrm{t}_-|^2 + |\mathrm{t}_+|^2) - (|\mathrm{r}_-|^2 + |\mathrm{r}_+|^2)} \tag{8}$$

where $A_\pm = 1 - |t_\pm|^2 - |r_\pm|^2$. In addition, we define the isolation ratio as $\imath = |t_-/t_+|$. In the case at hand, achieving a high isolation ratio will lead to high MCD, as seen from Equation (3). For instance, when illuminating one side (the "$+z$" direction) with RCP light, the response is $t_+$, while LCP light yields $t_-$. Conversely, illuminating from the opposite side ("$-z$" direction) with RCP light produces $t_-$, and with LCP, $t_+$. A high MCD means one polarization is mainly absorbed, and the other is not; the previously blocked polarization is not absorbed when the direction is reversed. Next, we look for the conditions to design a partial isolator for circularly polarized light, that is, a device that fully absorbs one polarization from one side and transmits it from the other.

We start by finding the conditions to achieve high isolation for circularly polarized light using the theoretical results obtained in the last section, that is, Equations (4)–(7). Thus, we aim to ensure the full absorption and full transmission of light of a given circular polarization incident on the metasurface from the two opposite directions. Without loss of generality, we determine these two conditions for the right-handed circular polarization (as shown below, the dual conditions will be automatically satisfied for the opposite polarization). Mathematically, the conditions read as

$$A_{\mathrm{R}}^{\mathrm{f}} = 1 - |t_{\mathrm{R-R}}^{\mathrm{f}}|^2 - |r_{\mathrm{L-R}}^{\mathrm{f}}|^2 = 1, \quad |t_{\mathrm{R-R}}^{\mathrm{b}}| = 1 \tag{9}$$

Naturally, they would lead to the scenario of maximization of the $\imath$ ratio. To simplify the derivation, in the following, the case where $r_d = 0$ and $t_d = 1$ is explored. Using Equations (4)–(7) and Equation (3), we can express absorption of the RCP light incident in the forward direction as $A_{\mathrm{R}}^{\mathrm{f}} = 1 - |t_+|^2 - |r_+|^2 = A_+$, which results in

$$\mathrm{A}_+ = \frac{2\gamma_m^+/\tau_m^+}{(\gamma_m^+ + 1/\tau_m^+)^2 + (\omega - \omega_m^+)^2} + \frac{2\gamma_e^+/\tau_e^+}{(\gamma_e^+ + 1/\tau_e^+)^2 + (\omega - \omega_e^+)^2} \tag{10}$$

To satisfy the first condition (maximization of $A_+$), the eigenfrequencies for the resonances of both parities have to be equal $\omega_m^+ = \omega_e^+ = \omega^+$, and the maximum will take place at the frequency $\omega = \omega^+$. To reach precisely unitary absorption, we should ensure $|r_+|^2 = 0$ and $|t_+|^2 = 0$. We study both cases separately and then combine the conditions. At the resonant frequency, $|r_+|^2 = 0$ is obtained if

$$\gamma_m^+\tau_m^+ = \gamma_e^+\tau_e^+ \tag{11}$$

This constraint leads to the condition of a Huygens' metasurface.[51] Furthermore, forcing separately that $|t_+|^2 = 0$ at the resonance frequency will yield

$$\frac{1}{\tau_m^+}\frac{1}{\tau_e^+} = \gamma_m^+\gamma_e^+ \tag{12}$$

Combining both Equations (11) and (12), we end up with the known condition of critical coupling that ensures full absorption of incoming energy at the resonance frequency

$$\frac{1}{\tau_m^+} = \gamma_m^+, \qquad \frac{1}{\tau_e^+} = \gamma_e^+ \tag{13}$$

This result is widely known for reciprocal metasurfaces and can be interpreted as a balance between the losses induced by the material and the scattering losses.[52] In contrast, in our case, the critical coupling condition holds at a given frequency only for one illumination direction. Substituting conditions in Equation (13) into Equation (10), we indeed obtain $A_+ = 1$.

In what follows, we additionally require zero reflection condition $|r_+(\omega)|^2 = |r_-(\omega)|^2 = 0$ for all frequencies $\omega$. Such a broadband Huygens' regime[53] has multiple practical advantages such as the possibility to cascade several metasurfaces and the minimization of parasitic interference. As is seen from Equation (6), broadband suppression of reflections for illuminations from both sides is achieved when we choose $\omega_m^- = \omega_e^- = \omega^-$ and additionally satisfy:

$$\gamma_m^+ = \gamma_e^+ = \gamma^+, \quad \tau_m^+ = \tau_e^+ = \tau^+, \quad \gamma_m^- = \gamma_e^- = \gamma^-, \quad \tau_m^- = \tau_e^- = \tau^- \tag{14}$$

Next, to satisfy the second condition in Equation (9) at a given frequency $\omega$, there are two possible *limiting* scenarios. The first one is to ensure full absorption for RCP light incident on the metasurface in the backward direction $A_{\mathrm{R}}^{\mathrm{b}} = 1 - |t_{\mathrm{R-R}}^{\mathrm{b}}|^2 - |r_{\mathrm{L-R}}^{\mathrm{b}}|^2 = A_-$ but occurring at a different frequency $\omega^- \neq \omega^+$. By decoupling the two resonance frequencies such that the spectral distance between them is much greater than their widths, that is, $|\omega^- - \omega^+| \gg |\gamma_{e,m}^+ + 1/\tau_{e,m}^+|$, we can asymptotically reach $|t_{\mathrm{R-R}}^{\mathrm{b}}| \approx 1$ at the frequency of $\omega^+$. This scenario is depicted in **Figure 5a**. Due to the condition in Equation (14), reflections are zero at all frequencies, while the absorption peaks for two light propagation directions are spectrally separated. To have complete absorption $A_-(\omega^-) = 1$, one needs to additionally satisfy $1/\tau^- = \gamma^-$.

The second limiting scenario for satisfying the condition in Equation (9) is when the metasurface is completely transparent at all frequencies (unitary transmission with an arbitrary phase)

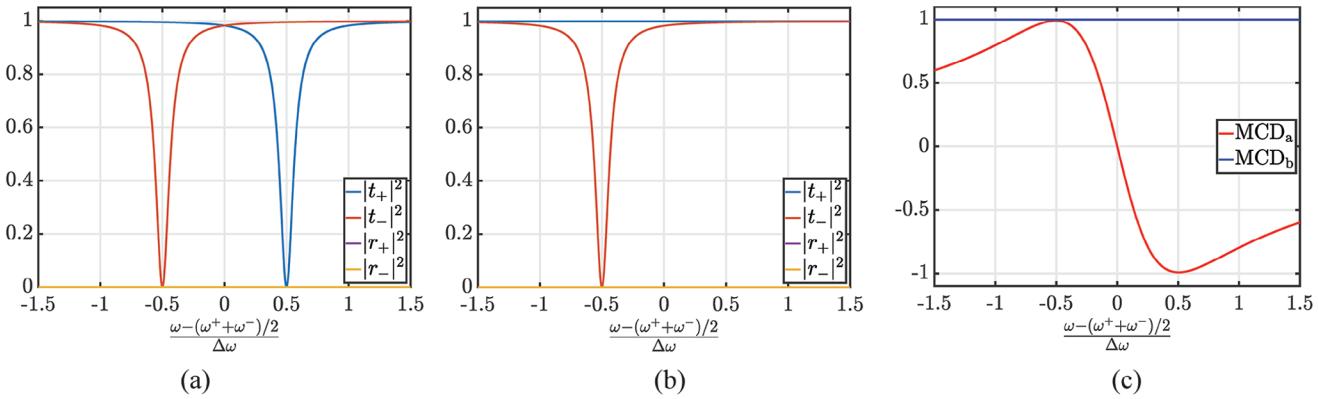


**Figure 5.** a) Reflectances and transmittances for an ideal metasurface exhibiting maximal isolation for circularly polarized light of a given handedness. The metasurface behaves as a broadband-matched resonant absorber, where the resonant frequency depends on the illumination direction. In this example, $\gamma^+ = \gamma^- = 1/\tau^+ = 1/\tau^- = \gamma$, $t_d = 1$, and $\Delta\omega = \omega^+ - \omega^- = 30\gamma$. The horizontal axis is normalized in such a way that its center corresponds to the average between $\omega^+$ and $\omega^-$. At frequency $\omega^+$, transmission for the backward propagating RCP light reaches $|t_-(\omega^+)|^2 = 0.996$. b) The same for a metasurface that exhibits no material loss for RCP (LCP) light when illuminated in the backward (forward) direction. c) MCD for the two limiting scenarios in (a) and (b).

for RCP light incident in the backward direction. This scenario is presented in Figure 5b. It can be achieved if $1/\tau^- = 0$.

As was mentioned above, at frequencies where the isolation ratio $\imath = |t_-/t_+|$ is high, the MCD is large. In Figure 5c, we plot the MCD parameter for the two above scenarios. While in the first scenario, the MCD approaches unit value at $\omega = \omega^+$, in the second scenario, it is a unit for all the frequencies due to its definition.

## 5. Ferrimagnetic Metasurface Realization

Using a metasurface with the geometry described in Figure 1 and ferrimagnetic material (Bi3YIG[43]) with a tensor given by Equation (1), the maximization of MCD and isolation properties studied theoretically in the last section can be applied. In the case of the real structure, the configuration for the resonances must be achieved by tweaking the geometrical parameters. Studying the behavior of the structure when there is no bias and no losses ($\varepsilon_{xy} = 0$ and $\varepsilon_{xx} = \varepsilon_{1r}$), it is apparent that the decay rates of the magnetic and electric resonances are intrinsically different, see Figure 2. However, both can be changed by tuning the asymmetry parameter $\Delta$. It must also be noted that the wavelength shift of the electric dipole resonances is noticeable when $\Delta$ is changed. In contrast, the magnetic dipole resonances shift much slower, as is seen in Figures 2c and 3. The magnetic bias will split each of the magnetic and electric dipole resonances into two, one coupling to the incident right-handed circularly polarized light in the forward direction (plus sign in the vector basis convention), and the other coupling to the left-handed circularly polarized light in the forward direction (minus sign in the vector basis convention).[46] By introducing losses, the behavior of the resonances holds, but the resonances suffer a drop in quality factor and do shift.

The final design uses optimization techniques for the geometrical parameters and the aforementioned knowledge to maximize the MCD. Analyzing the qualitative picture in Figure 5a, one can find that the relative magnitude of the off-diagonal component of the permittivity tensor $\varepsilon_{xy}/\varepsilon_{xx}$ is proportional to the distance in wavelength/frequency between the nondegenerated resonances after the split. Thus, there is a trade-off for designing a metasurface with a high isolation ratio at a given frequency: the smaller the value of $\varepsilon_{xy}/\varepsilon_{xx}$ is, the higher the quality factors of the exploited resonances must be. Since in optics, magneto-optical effects are very weak in all accessible natural materials ($|\varepsilon_{xy}| << |\varepsilon_{xx}|$), obtaining strong isolation needs structures with very high-quality factors. Although conventional Huygens' metasurfaces with magneto-optical inclusions can support relatively high-$Q$-factor resonances,[17] their reachable isolation ratios are limited. Using the proposed metasurface with quasi-BICs, we can reach high isolation in a sub-wavelength geometry even when using conventional low-loss magneto-optical materials. Moreover, quasi-BIC resonances provide us with an additional knob for the metasurface design. The geometrical perturbation parameter $\Delta$ can be tuned in a continuous range prior to metasurface fabrication. By controlling $\Delta$, we can straightforwardly control the quality factor and tune the decay rates and losses in the metasurface ($Q \simeq 1/\Delta^2$). We chose the geometrical parameters of the metasurface as mentioned in the caption of **Figure 6**.

The simulated scattering parameters of the metasurface, when illuminated normally with circularly polarized light, are shown in Figure 6a. The CMT fitting is also shown in the same plot, accurately modeling the simulated data. A maximum for the MCD is obtained at $\lambda = 648.5$ nm, reaching $|\text{MCD}| = 0.996$, as shown in Figure 6b. At the same wavelength, $|t_+|$ is almost fully suppressed. Moreover, the amount of energy transmitted forward with LCP polarization reaches 73.90%, while only 0.12% of LCP light would be transmitted in the backward direction. The raw contrast between transmittances $|t^{\text{f}}_{L-L}/t^{\text{b}}_{L-L}|^2 = |t_-/t_+|^2 = \imath^2 \approx 625$, which can be expressed as a 27.89 dB isolation ratio. The energy with a defined circular polarization can go through the device in one direction while being absorbed in the opposite direction.

Finally, in Figure 6c, we plot the Faraday rotation angle $\theta$ and ellipticity $\epsilon$ versus wavelength for the designed metasurface. We use the conventional definition for the rotation angle $\theta = 1/2 \arctan[2\Re(\chi)/(1-|\chi|^2)]$, where $\chi = E^{\text{tr}}_y/E^{\text{tr}}_x$. Where $\Re$ denotes the real part of a function. The ellipticity $\epsilon$ is defined as the

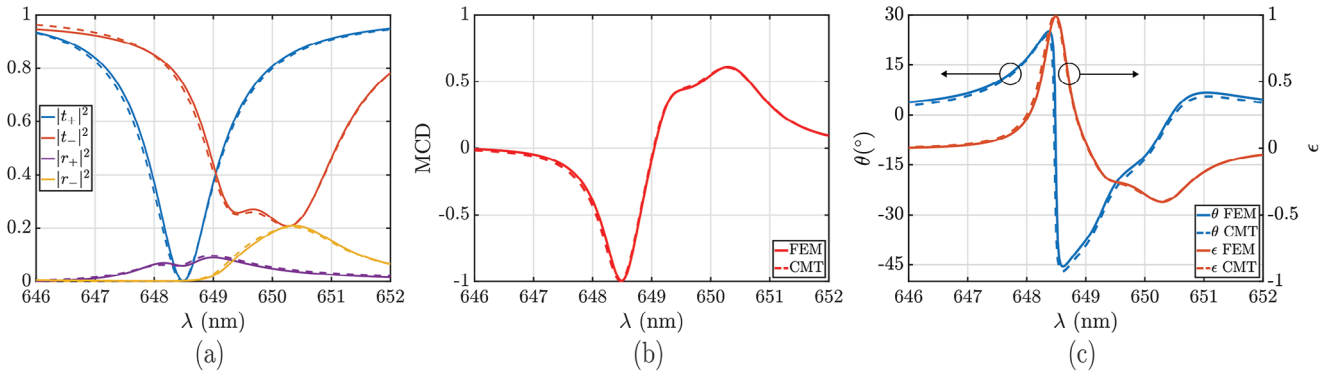


**Figure 6.** a) Reflectances and transmittances of the optimized metasurface when illuminated with circularly polarized light at normal incidence. The CMT fit is plotted with a dashed line with the same color as the simulated data (denoted as FEM). b) MCD of the metasurface. c) The Faraday rotation angle and ellipticity of the designed metasurface versus the wavelength. The geometrical parameters of the structure are $w = 430$ nm, $h = 135.6$ nm, $l = 269.2$ nm, and $\Delta = 24.7$ nm. The values obtained for the CMT fit are $\omega_m^- = 2896.3$ THz, $\omega_m^+ = 2904.8$ THz, $\omega_e^- = 2901.5$ THz and $\omega_e^+ = 2904.8$ THz for the eigenfrequencies; $\gamma_m^- = \gamma_m^+ = \gamma_m = 2.2$ THz, $\gamma_e^- = \gamma_e^+ = \gamma_e = 0.8$ THz for the scattering decay rates; $1/\tau_m^- = 2.25$ THz, $1/\tau_e^- = 1.69$ THz and $1/\tau_m^+ = 1/\tau_e^+ = 1.42$ THz for the absorption decay rates. Finally, $t_d = 0.998$ is used as the direct pathway parameter.

ratio between the size of the major and the minor axis of the polarization ellipse of transmitted light. At $\lambda = 648.5$ nm the ellipticity reaches almost unity. This occurs because almost all of the transmitted light is circularly polarized with left-handedness. On the other hand, at $\lambda = 649.05$ nm where ellipticity is equal to zero, the metasurface rotates linearly polarized light at an angle $\theta = 36.4^\circ$ with the transmittance $|t|^2 = 40.5\%$. The obtained values of the rotation angle and ellipticity are high, taking into account the subwavelength thickness of the metasurface ($h/\lambda = 0.21$) and the realistic material parameters used. We can also estimate the effective Verdet constant of the metasurface $V = \theta/(\mu_0 H_0 h)$.[6] Taking $\mu_0 H_0 = 0.66$ T from ref. [43], the Verdet constant reaches the maximum value of $V = 7.12 \times 10^6$ rad T$^{-1}$ m$^{-1}$, which exceeds the value for thin-film of conventional MO materials by 3–4 orders of magnitude.[6] Such enhancement of the MO properties is enabled by the use of quasi-BICs in our geometry.

## 6. Conclusions

We have developed a metasurface made out of a ferrimagnetic material and based on quasi-BIC resonances that, with the use of orthogonal pairs of resonances with electric and magnetic nature, can achieve high MCD combined with strong isolation for circular polarization. The device acts with this configuration as a partial isolator, as the transmission for the non-blocked polarization is maximized. In addition, by matching the resonance amplitudes and phases, it is possible to use the quasi-BIC-empowered metasurface to enhance the Faraday effect of the structure. An unprecedented figure of merit is obtained using this approach. All of the above has been designed using a realistic material (Bi3YIG), experimentally characterized, and with noticeable losses. Importantly, it is not necessary to bias the metasurface with an external magnet. Ferri- and ferromagnetic nanodisks can sustain strong spontaneous magnetization when they are fabricated in a single-domain magnetic state.[54] The direction of this magnetization is typically along the nanodisk axis and is governed by the shape and magnetocrystalline anisotropies.[55]

The finite-element-method simulations have been supported with a CMT description of the metasurface. This phenomenological theoretical model has been useful in predicting and explaining the capabilities of the device. Furthermore, it supports the observed enhancement of the Faraday effect and proves the use of BICs as a path to control and enhance MO effects. The realization of a Faraday rotator can lead to the creation of a compact isolator using two linear polarizers in the famous Faraday-isolator architecture. Although the size of the isolator, if not fabricated in a single-domain magnetic state, would be limited by the magnet creating the external magnetic field, many optical components are not affected by external magnetic fields and could fit in the same space.

In order to design a polarization-insensitive partial optical isolator, one needs to additionally break the inversion (parity) symmetry that is currently present in the metasurface design. This can be straightforwardly achieved using a conventional approach by introducing two circular polarizers (with the same handedness) around the metasurface (e.g., the Supplementary Information in ref. [41] and Section S6, Supporting Information.)

## Supporting Information

Supporting Information is available from the Wiley Online Library or from the author.

## Acknowledgements

This research was supported by the Beatriz Galindo excellence grant (grant No. BG-00024), the Spanish National Research Council (grant No. PID2021-128442NA-I00), and the Academy of Finland (Project No. 356797).

## Conflict of Interest

The authors declare no conflict of interest.

## Data Availability Statement

The data that support the findings of this study are available from the corresponding author upon reasonable request.

## Keywords

bound states in the continuum, Faraday rotation, magneto-optical effect, metasurfaces

Received: June 19, 2023
Revised: October 2, 2023
Published online: November 15, 2023

[1] O. Quevedo-Teruel, H. Chen, A. Díaz-Rubio, G. Gok, A. Grbic, G. Minatti, E. Martini, S. Maci, G. V. Eleftheriades, M. Chen, N. I. Zheludev, N. Papasimakis, S. Choudhury, Z. A. Kudyshev, S. Saha, H. Reddy, A. Boltasseva, V. M. Shalaev, A. V. Kildishev, D. Sievenpiper, C. Caloz, A. Al, Q. He, L. Zhou, G. Valerio, E. Rajo-Iglesias, Z. Sipus, F. Mesa, R. Rodríguez-Berral, F. Medina, et al., *J. Opt. (Bristol, U. K.)* **2019**, *21*, 073002.
[2] K. Singh, F. Ahmed, K. Esselle, *Crystals* **2022**, *12*, 1769.
[3] F. Ding, A. Pors, S. I. Bozhevolnyi, *Rep. Prog. Phys.* **2018**, *81*, 026401.
[4] H. T. Chen, A. J. Taylor, N. Yu, *Rep. Prog. Phys.* **2016**, *79*, 076401.
[5] D. Jalas, A. Petrov, M. Eich, W. Freude, S. Fan, Z. Yu, R. Baets, M. Popović, A. Melloni, J. D. Joannopoulos, M. Vanwolleghem, C. R. Doerr, H. Renner, *Nat. Photonics* **2013**, *7*, 579.
[6] V. S. Asadchy, M. S. Mirmoosa, A. Díaz-Rubio, S. Fan, S. A. Tretyakov, *Proc. IEEE* **2020**, *108*, 1684.
[7] E. Lifshitz, L. Pitaevskii, *Physical Kinetics, Course of Theoretical Physics*, Vol. *10*, Elsevier Science, Amsterdam **1995**.
[8] V. I. Belotelov, I. A. Akimov, M. Pohl, V. A. Kotov, S. Kasture, A. S. Vengurlekar, A. V. Gopal, D. R. Yakovlev, A. K. Zvezdin, M. Bayer, *Nat. Nanotechnol.* **2011**, *6*, 370.
[9] M. Inoue, K. N. Arai, T. Fujii, M. Abe, *J. Appl. Phys.* **1999**, *85*, 5768.
[10] E. Takeda, N. Todoroki, Y. Kitamoto, M. Abe, M. Inoue, T. Fujii, K. Arai, *J. Appl. Phys.* **2000**, *87*, 6782.
[11] M. J. Steel, M. Levy, R. M. Osgood, *IEEE Photonics Technol. Lett.* **2000**, *12*, 1171.
[12] G. Armelles, A. Cebollada, A. García-Martín, M. U. González, *Adv. Opt. Mater.* **2013**, *1*, 10.
[13] J. Y. Chin, T. Steinle, T. Wehlus, D. Dregely, T. Weiss, V. I. Belotelov, B. Stritzker, H. Giessen, *Nat. Commun.* **2013**, *4*, 1599.
[14] N. MacCaferri, X. Inchausti, A. García-Martín, J. C. Cuevas, D. Tripathy, A. O. Adeyeye, P. Vavassori, *ACS Photonics* **2015**, *2*, 1769.
[15] V. S. Asadchy, C. Guo, B. Zhao, S. Fan, *Adv. Opt. Mater.* **2020**, *8*, 2000100.
[16] Z. Khaghani, M. H. Farzad, A. Asgari, *Opt. Quantum Electron.* **2022**, *54*, 645.
[17] A. Christofi, Y. Kawaguchi, A. Alù, A. B. Khanikaev, *Opt. Lett.* **2018**, *43*, 1838.
[18] S. Xia, D. O. Ignatyeva, Q. Liu, J. Qin, T. Kang, W. Yang, Y. Chen, H. Duan, L. Deng, D. Long, M. Veis, V. I. Belotelov, L. Bi, *ACS Photonics* **2022**, *9*, 1240.
[19] M. G. Barsukova, A. I. Musorin, A. S. Shorokhov, A. A. Fedyanin, *APL Photonics* **2019**, *4*, 016102.
[20] D. O. Ignatyeva, D. Karki, A. A. Voronov, M. A. Kozhaev, D. M. Krichevsky, A. I. Chernov, M. Levy, V. I. Belotelov, *Nat. Commun.* **2020**, *11*, 5487.
[21] S. A. Tretyakov, A. J. Viitanen, *J. Electromagn. Waves Appl.* **2000**, *14*, 1159.
[22] A. S. Kupriianov, Y. Xu, A. Sayanskiy, V. Dmitriev, Y. S. Kivshar, V. R. Tuz, *Phys. Rev. Appl.* **2019**, *12*, 014024.
[23] C. W. Hsu, B. Zhen, A. D. Stone, J. D. Joannopoulos, M. Soljacic, *Nat. Rev. Mater.* **2016**, *1*, 16048.
[24] Y. He, G. Guo, T. Feng, Y. Xu, A. E. Miroshnichenko, *Phys. Rev. B* **2018**, *98*, 161112.
[25] J. Lee, B. Zhen, S. L. Chua, W. Qiu, J. D. Joannopoulos, M. Soljačić, O. Shapira, *Phys. Rev. Lett.* **2012**, *109*, 067401.
[26] Y. Tang, Y. Liang, J. Yao, M. K. Chen, S. Lin, Z. Wang, J. Zhang, X. G. Huang, C. Yu, D. P. Tsai, *Laser Photonics Rev.* **2023**, *17*, 2200597.
[27] M. V. Gorkunov, A. A. Antonov, Y. S. Kivshar, *Phys. Rev. Lett.* **2020**, *125*, 093903.
[28] M. V. Gorkunov, A. A. Antonov, V. R. Tuz, A. S. Kupriianov, Y. S. Kivshar, *Adv. Opt. Mater.* **2021**, *9*, 2100797.
[29] X. Zong, L. Li, Y. Liu, *New J. Phys.* **2023**, *25*, 023020.
[30] J. Tian, Q. Li, P. A. Belov, R. K. Sinha, W. Qian, M. Qiu, *ACS Photonics* **2020**, *7*, 1436.
[31] K. Koshelev, S. Lepeshov, M. Liu, A. Bogdanov, Y. Kivshar, *Phys. Rev. Lett.* **2018**, *121*, 193903.
[32] P. Yu, A. S. Kupriianov, V. Dmitriev, V. R. Tuz, *J. Appl. Phys.* **2018**, *125*, 143101.
[33] K. Sakoda, *Phys. Rev. B* **1995**, *52*, 7982.
[34] A. C. Overvig, S. C. Malek, M. J. Carter, S. Shrestha, N. Yu, *Phys. Rev. B* **2020**, *102*, 035434.
[35] G. Y. Chen, W. X. Zhang, X. D. Zhang, *Opt. Express* **2019**, *27*, 16449.
[36] A. M. Chernyak, M. G. Barsukova, A. S. Shorokhov, A. I. Musorin, A. A. Fedyanin, *JETP Lett.* **2020**, *111*, 46.
[37] D. R. Abujetas, N. de Sousa, A. García-Martín, J. M. Llorens, J. A. Sánchez-Gil, *Nanophotonics* **2021**, *10*, 4223.
[38] W. Suh, Z. Wang, S. Fan, *IEEE J. Quantum Electron.* **2004**, *40*, 1511.
[39] Z. Zhao, C. Guo, S. Fan, *Phys. Rev. A* **2019**, *99*, 033839.
[40] M. Chen, M. Kim, A. M. Wong, G. V. Eleftheriades, *Nanophotonics* **2018**, *7*, 1207.
[41] M. Lawrence, J. A. Dionne, *Nat. Commun.* **2019**, *10*, 3297.
[42] J. Hu, M. Lawrence, J. A. Dionne, *ACS Photonics* **2020**, *7*, 36.
[43] E. Jesenska, T. Yoshida, K. Shinozaki, T. Ishibashi, L. Beran, M. Zahradnik, R. Antos, M. Kučera, M. Veis, *Opt. Mater. Express* **2016**, *6*, 1986.
[44] M. Zhou, D. Liu, S. W. Belling, H. Cheng, M. A. Kats, S. Fan, M. L. Povinelli, Z. Yu, *ACS Photonics* **2021**, *8*, 2265.
[45] K. Sakoda, *Optical Properties of Photonic Crystals*, Springer, Berlin, Heidelberg, **2005**.
[46] K. Fang, Z. Yu, V. Liu, S. Fan, *Opt. Lett.* **2011**, *36*, 4254.
[47] J. A. Álvarez-Sanchis, B. Vidal, S. A. Tretyakov, A. Díaz-Rubio, *Phys. Rev. Appl.* **2023**, *19*, 014009.
[48] A. V. Kondratov, M. V. Gorkunov, A. N. Darinskii, R. V. Gainutdinov, O. Y. Rogov, A. A. Ezhov, V. V. Artemov, *Phys. Rev. B* **2016**, *93*, 195418.
[49] C. Caloz, A. Sihvola, *arXiv:1903.09087*, **2019**.
[50] S. E. Braslavsky, *Pure Appl. Chem.* **2007**, *79*, 293.
[51] M. Chen, M. Kim, A. M. Wong, G. V. Eleftheriades, *Nanophotonics* **2018**, *7*, 1207.
[52] Y. Park, V. S. Asadchy, B. Zhao, C. Guo, J. Wang, S. Fan, *ACS Photonics* **2021**, *8*, 2417.
[53] V. S. Asadchy, I. A. Faniayeu, Y. Ra'di, S. A. Khakhomov, I. V. Semchenko, S. A. Tretyakov, *Phys. Rev. X* **2015**, *5*, 031005.
[54] J. M. D. Coey, *Magnetism and Magnetic Materials*, Cambridge University Press, Cambridge **2010**.
[55] S. S. Jazi, I. Faniayeu, R. Cichelero, D. C. Tzarouchis, M. M. Asgari, A. Dmitriev, S. Fan, V. Asadchy, *arXiv:2307.09275*, **2023**.